

Real-time 3D localization of RFID-tagged products by ground robots and drones with commercial off-the-shelf RFID equipment: Challenges and Solutions

Anastasios Tzitzis*, Alexandros Filotheou*, Stavroula Siachalou*, Emmanouil Tsardoulis*, Spyros Megalou*, Aggelos Bletsas⁺, Konstantinos Panayiotou*, Andreas Symeonidis*, Traianos Yioultsis*, Antonis G. Dimitriou*

*School of Electrical and Computer Engineering, Aristotle University of Thessaloniki, Thessaloniki, Greece

⁺School of Electrical and Computer Engineering, Technical University of Crete, Chania, Greece

antodimi@ece.auth.gr

Abstract—In this paper we investigate the problem of localizing passive RFID tags by ground robots and drones. We focus on autonomous robots, capable of entering a previously unknown environment, creating a 3D map of it, navigating safely in it, localizing themselves while moving, then localizing all RFID tagged objects and pinpointing their locations in the 3D map with cm accuracy. To the best of our knowledge, this is the first paper that presents the complex joint problem, including challenges from the field of robotics - *i*) sensors utilization, *ii*) local and global path planners, *iii*) navigation, *iv*) simultaneous localization of the robot and mapping - and from the field of RFIDs - *vi*) localization of the tags. We restrict our analysis to solutions, involving commercial UHF EPC Gen2 RFID tags, commercial off-the-self RFID readers and 3D real-time-only methods for tag-localization. We briefly present a new method, suitable for real-time 3D inventorying, and compare it with our two recent methods. Comparison is carried out on a new set of experiments, conducted in a multipath-rich indoor environment, where the actual problem is treated; i.e. our prototype robot constructs a 3D map, navigates in the environment, continuously estimates its poses as well as the locations of the surrounding tags. Localization results are given in a few seconds for 100 tags, parsing approximately 100000 measured samples from 4 antennas, collected within 4 minutes and achieving a mean 3D error of 25cm, which includes the error propagating from robotics and the uncertainty related to the "ground truth" of the tags' placement.

Index Terms—RFID, robotics, localization, inventorying

I. INTRODUCTION

In the context of our project "RELIEF" [1], we focus on the problem of continuous inventorying in large warehouses and retail-stores. All target products are tagged with passive UHF EPC Gen2 RFID tags. A fixed reader-antenna network, continuously monitoring the entire area, would require a prohibitive installation cost. Instead, we have designed and constructed two prototype RFID-equipped robots (see Fig. 1) and a drone

(Fig. 2), capable to carry out the task. The goals of the robots are to be able to construct a map of the "a priori" unknown environment, to navigate autonomously and safely inside it, to interpret their own pose (position and direction) and to identify and rapidly locate all RFID tagged items with cm accuracy and project their locations in the previously created 3D map. In simple words, one would "Plug and Play" a robot in the area and expect a 3D map of the space along with the products. Typical applications may include querying a database for a specific product and get a 3D result pinpointing its location on the map, real-time notifications on the locations of sensitive products, e.g. expired products inside a supermarket, real-time localization of books inside a library etc.

Our robots are not the first ones in the market to address the inventorying problem. Existing commercial robots are "Tory" [2], "AdvanRobot" [3], "StockBot" [4] and more. All aforementioned robots are also designed to autonomously navigate in unknown environments and probably to localize the surrounding tags. Localization of the tags is an inherent property of the antenna-reader system; i.e. when a tag is successfully interrogated, it belongs to the read-region of the specific antenna, but this property will give a poor accuracy of meters. So the real benchmark becomes how well each robot addresses its complex mission. Our target is to localize all products with a mean 3D error of less than 10cm (comparable to the dimensions of the tag) and accomplish that task in real-time, without the use of custom wide-band technology.

The typical available physical quantities for localization of UHF EPC Gen2 RFID tags are *i*) the backscattered power, usually referred as RSSI and *ii*) the phase of the backscattered signal of each tag. In contrast to RSSI, which can be directly mapped into distance, a single phase sample is useless for localization, due to the 2π ambiguity of phase measurements. However, the robot allows for a dense collection of successive RSSI and phase measurements from different locations, thus forming a "Synthetic Aperture" or "Virtual Antenna Array". In this perspective, the phase information represents a better metric (over RSSI) for localization of the tag, given its tolerance

This research has been co-financed by the European Union and Greek national funds through the Operational Program Competitiveness, Entrepreneurship and Innovation, under the call RESEARCH –CREATE – INNOVATE (project code:T1EDK-03032)

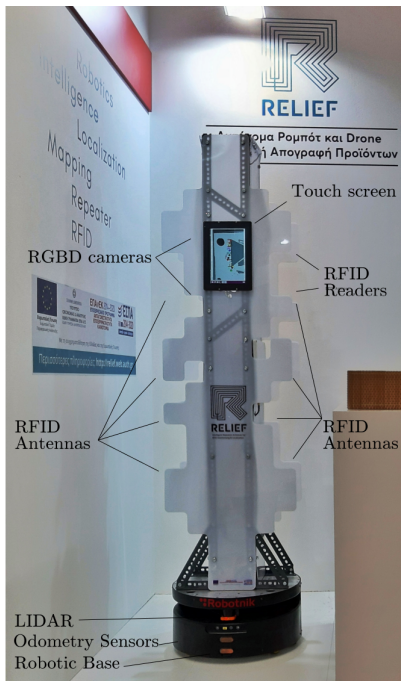


Fig. 1: Photo of "Frida" from a recent international exhibition.

on the tag's antenna polarization, detuning or partial blockage, while experiencing smaller variations due to multipath.

As a consequence, the most accurate localization algorithms are based on phase measurements collected along a Synthetic Aperture, a technique known from radar systems, which is now applied in RFID localization technology [5] - [9]. However, in all cases calculations are carried out on a grid. As a result, all algorithms fail to accomplish real-time results for realistic tag populations and 3D spaces, due to the size of the grid. Two different approaches were presented in [10], [11]; yet [11] requires functionality of the tag's antenna over large bandwidth and it cannot be applied in real-time for large populations, while [10] represents an interesting alternative to the problem, though it should be extended in 3D. Recently, we have introduced "Phase ReLock", [12] - [14], a method which transforms the original optimization problem into a new equivalent form, which can be solved **rapidly** by standard iterative optimization techniques (instead of searching on a grid).

The aforementioned localization methods require knowledge of the exact trace of the robot. However, this is not always possible. For instance, a lightweight drone, suitable for indoor warehouse monitoring may not be able to carry the sensing-equipment for localization of its own pose (a lightweight 360° lidar weighs more than 500g). Under such circumstances, a reasonable alternative is to explore fingerprinting methods, where localization of the unknown tags is carried out by evaluating the resemblance of their measured characteristics (RSSI and phase) with measurements of reference tags, placed at known locations, collected from the same equipment at the same time. Starting from "Landmarc" [15], we have developed



Fig. 2: Photo of the RFID equipped drone.

a fingerprinting method exploiting the RSSI [16] and the phase [17] measurements, while we have proposed real-time performance evaluation by further exploiting the reference tags.

In addition we focus on problems related to robotics; map construction, global/local planners [30], sensors' performance, localization of robot and navigation.

In this paper, in contrast to prior art, where the poses of the robot are taken for granted, we present an overview of the problem, starting from robotics and the related uncertainties, which affect the accuracy of the tag's positioning. Secondly, we briefly introduce a prototype real-time tag-localization method, where the phase-unwrapped sequence of samples becomes the input to an over-determined linear system, which is rapidly solved to extract the location of each tag. The new method performs even faster than "Phase ReLock", [12] - [14], with comparable accuracy, achieving localization of 100 tags in just 6s- the estimation time is orders of magnitude smaller than the duration of the measurements by the moving robot, which lasted for minutes. Thirdly, we compare the performance of the proposed methods in a new set of experiments involving tags arranged in different **3D configurations**. In these experiments, the map is created during each experiment, the robot navigates autonomously, the poses/locations of the robot are estimated (and not considered known) and the locations of the tags in the surrounding area are updated dynamically. Mean 3D error, including the robotics SLAM error, in the order of **25cm** is achieved, which is comparable to the dimensions of the tags (10cm) and the uncertainty related to the ground-truth of the tags' actual locations.

II. ROBOT - REQUIREMENTS AND CONSTRAINTS

The phrase "RFID-tag localization" implies that, within the environment where tags are situated, there exists a frame of reference in which their location can be inferred. In practice, the inference made requires the use of the sensor's pose relative to the same frame of reference. In situations where the sensor is mounted at a fixed pose on a mobile robot, as is customary in most mobile robotics applications, inferring the sensor's pose is mediated by inferring the robot's pose, which, in GPS-denied environments such as indoors, can usually only be estimated, in contrast to being measured. In

mobile robotics, the estimation of a robot’s pose using only equipment mounted on the robot is called Robot localization and, together with mapping, i.e. “Simultaneous localization and Mapping” (SLAM), they comprise its two fundamental tasks. Accurate robot localization is of paramount importance for the tag-localization problem, since most methods assume the reader-antennas’ locations as known. A robot-localization error propagates into the tag-localization estimation.

A. Robot Localization

The task of robot localization assumes the existence of a map of the robot’s surroundings, and it is comprised of two discrete problems. The first constitutes the estimation of the robot’s initial resting pose in the map and is termed “the Global localization problem”. The second is the estimation of the robot’s pose through time, given the robot’s initial resting pose and is called “the Pose-Tracking problem”. In the case of terrestrial robots, and depending on the robot’s sensors, a 2D map is sufficient to estimate the pose $p(x, y, \theta)$ of the robot in the 2D plane. In the case of drones, a 3D map is necessary, where the full $p(x, y, z, roll, pitch, yaw)$ pose is required.

Let us now consider the problem of pose tracking. The simplest way of estimating the robot’s pose through time is integrating the motor’s control commands into the kinematic or dynamic model of the robot, enhanced by (non-exteroceptive) sensors (e.g. counting the number of wheels’ revolutions). Due to the model’s inescapable mismatch to reality, wheel slippage in terrestrial robots, input noise, saturation, and other sources of error, the uncertainty of the robot’s pose grows without limit over time, eventually rendering pose estimation meaningless [19]. Consequently, the pose of the RFID sensor becomes unattainable, and therefore RFID-tag localization impossible. The only solution to improving the accuracy is to integrate sensors of the environment onto the robot (exteroceptive). The simplest sensor could be a conventional RGB camera. Through it, one can detect features in the robot’s environment and match them to features of the environment’s map.

More recently, the RGB camera was enhanced with the addition of *depth* information, [18]. Images captured through RGBD cameras convey and encode in each pixel the colour and depth content of the environment within the sensor’s field of view. Notwithstanding both sensors’ advantage of conveying rich information, both suffer from causes particular either to environment conditions or their systemic idiosyncrasy [20]- [22]. These pitfalls, along with the large volume of data to be processed, results in low-frequency pose updates and rather large uncertainty in pose estimation [23], [24], consequently propagating to rather crude RFID sensor pose estimates. In general, the above have led the current state-of-the-art to utilise RGBD sensors in a subsidiary capacity as regards localization, having a range-finder sensor act as the primary source of information from the environment.

A range-finder sensor measures its distance to objects in the environment at equiangular intervals over a range of up to 2π rad. Its encoding of the sense of depth (unlike RGB camera sensors), large range (greater than RGBD cameras),

real-time operational frequency, millimetre accuracy, minimal bandwidth needed, and virtually no need for preprocessing has made it the de facto sensor used for mobile robot localization. Even range-finders are susceptible to errors, since they usually operate with infrared light beams, thus the distances measured are far from correct when the environment contains transparent or highly reflective surfaces (glass, mirrors, and screens, among others).

Typically, the most accurate results are obtained when encoder measurements are fused with measurements from the range-finder(s) by using a Kalman [25] or Particle filter [19], [26]- [27]. These filters are utilised in robot localization due to their ability to track the pose of a robot while accommodating pose and sensor measurement uncertainty, and hence their robustness to various sources of error. In our work we use particle filters, a technique resting on the probabilistic Monte Carlo Localisation (MCL) approach [28]. The nature of MCL allows them to represent the uncertainty in the robot’s pose by maintaining a set of hypotheses (called particles) not bound to a unimodal probability density function. Among others, this representation allows a particle filter to globally localise a robot and keep track of pose ambiguities until being able to resolve them, by virtue of being able to represent arbitrarily complex probability densities.

Particle filters recursively estimate the posterior of a robot’s pose as follows:

$$p(\mathbf{x}_t | \mathbf{z}_{1:t}, \mathbf{u}_{0:t-1}, M) \propto \int_{\mathbf{x}'} p(\mathbf{x}_t | \mathbf{x}', \mathbf{u}_{t-1}) \cdot p(\mathbf{x}' | \mathbf{z}_{1:t-1}, \mathbf{u}_{0:t-2}, M) d\mathbf{x}' \quad (1)$$

Here, the pose of the robot at time t is denoted by \mathbf{x}_t ; $\mathbf{u}_{0:t-1}$ is the sequence of motion commands executed by the robot, and $\mathbf{z}_{0:t}$ is the sequence of observations made by the robot, obtained by 2D range scanners, cameras, sonars or other sensors; M is the map representing the environment in which the robot moves. The motion model $p(\mathbf{x}_t | \mathbf{x}_{t-1}, \mathbf{u}_{t-1})$ denotes the probability that, at time t , the robot ends up in pose \mathbf{x}_t given that it executes the motion command \mathbf{u}_{t-1} while posed at \mathbf{x}_{t-1} at time $t - 1$. The observation model $p(\mathbf{z}_t | \mathbf{x}_t, M)$ denotes the likelihood of making the observation \mathbf{z}_t while posed at \mathbf{x}_t . Figure 3 shows the progressive convergence of hypotheses during pose tracking when a particle filter using measurements of a range-finder is used to perform localization.

Coming back to the problem of global localization, it is now evident that it cannot be performed without the use of sensors that encode information about the robot’s environment. We are currently investigating ways of solution to the global localization problem that exploit RFID technology.

B. Simultaneous Localization and Mapping

One crucial phrase of the previous description about localization was “*assumes the existence of a map of the robot’s surroundings*”. Unfortunately, this assumption is almost never valid, since no blueprints of the environment exist a priori, thus a SLAM (Simultaneous Localization and Mapping) should

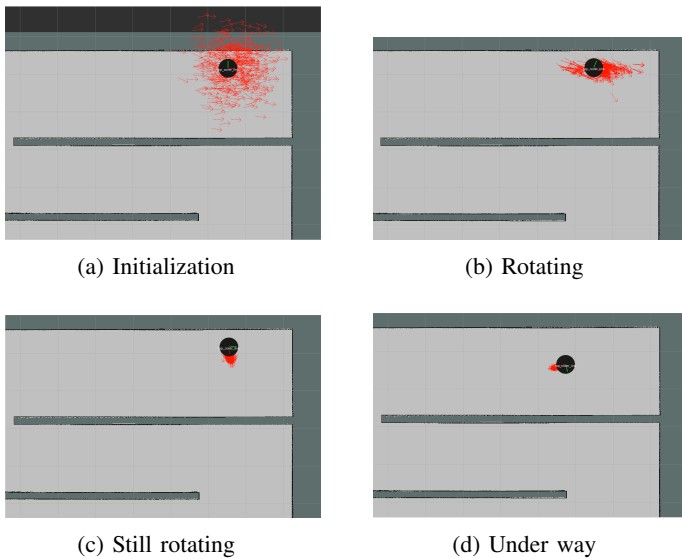


Fig. 3: Visualization of robot pose estimation during pose tracking with the use of a particle filter (particles, shown in red) utilising measurements off a range finder.

be deployed beforehand. SLAM algorithms keep track of the robot's pose in the map they concurrently construct, a problem usually described as "chicken or egg", since a correct map is needed to perform localization and an accurate pose is needed for a sound map.

SLAM is usually probabilistically solved using a Bayes filter in the form of either Kalman or particle filters, by utilizing distance or image sensors, and produce either metric or feature-based maps. In order to perform localization in a SLAM-generated map, the map has to be metric, i.e. each cell in 2D, or voxel in 3D, has to represent a specific area or volume in the real world. When two-dimensional metric maps are concerned, they are represented as Occupancy Grid Maps - OGMs [19], meaning that a map is an assemble of cells comprising a grid, each of which represents an area in the real world and contains a probability of this area to be occupied by an obstacle. Similarly, in the 3D case, the usual spatial representation is an Octomap [29], which contains voxels (3D cells), again containing occupancy probabilities.

Sensors' noise gravely affects the quality of the final map. If the distance sensors provide erroneous data, or if the robot moves abruptly and affects the chosen SLAM algorithm's functionality, the result is a disfigured map. State-of-the art SLAM algorithms cannot represent the environment correctly, thus any discrepancies between the generated map and the real environment introduce extra noise in the localization process. Another source of uncertainty is the nature of the grid-based representation itself. Each grid consists of cells, which have predefined dimensions (also known as map resolution). This usually ranges from 5cm to 50cm, depending on the total area we want to be mapped. Therefore, a e.g. 10cm \times 10cm cell may contain both free space and the edge of an obstacle, nevertheless it is represented by a single number in the OGM,

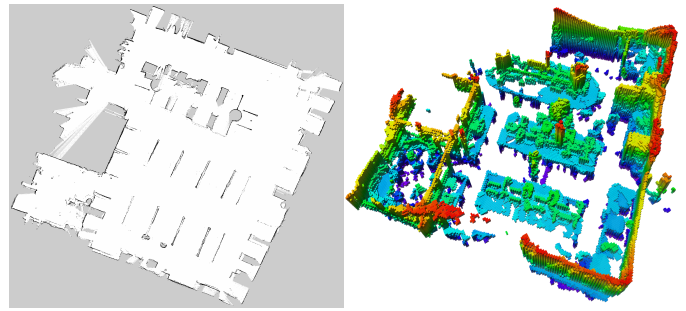


Fig. 4: 2D (Left) and 3D (Right) map created by "Frida" during an experiment.

fact that leads to even poorer performance in localization. Currently 2D SLAM algorithms greatly outperform 3D ones, since the dimensionality increase adds a great burden in CPU and memory requirements. Thus, when drones are concerned which must use 3D maps for their localization, larger errors are expected, due to the low resolution of the map they use to localize themselves. This error is propagated in the RFID localization, as explained earlier. Fig. 4 (left) shows the 2D map, using a range-finder sensor, created during an experiment in the lab, while Fig. 4 (right) shows the 3D map of the same environment built with the use of 3 RGBD cameras.

C. Navigation

In principle, robot navigation is carried out in either of two ways: by teleoperation or by the robot itself (autonomous). Autonomous robot navigation implies the existence of an end: that can be the robot reaching a target pose in the map, or the covering of some portion of the map (possibly its entirety), all while satisfying input, state, collision avoidance, or other set constraints. In the context of robotics, covering can be defined in terms of either the robot's footprint or the field of view of some sensor it employs. Two operators are required for autonomous robot navigation: *i*) a "global planner"; it constructs a connected path from one point of the map to another (from the robot's starting location to its target location), and *ii*) a "local planner"; it directs the robot's motors into following that path as closely as possible without violating any set constraints. The two operators work in tandem, waiting for a user-supplied target in the case where the robot is tasked to reach a specific pose, or a robot-supplied target, in the case where higher-level tasks, such as coverage of a portion of the map, are demanded. In [30] we have performed a comparative study of performance between global and local planners and their combinations. In the course and context of our project we have singled-out the NF1 navigation function approach [31] as a viable global planner, and, for a local planner, the flexible Timed-Elastic-Band approach [32], [33].

During navigation, when the map is expressed in two dimensions, navigation may still fail. One of the reasons may be inconsistencies between the obstacles depicted in the SLAM-generated map and the real ones, since environments are typically packed with movable or moving objects. Therefore,

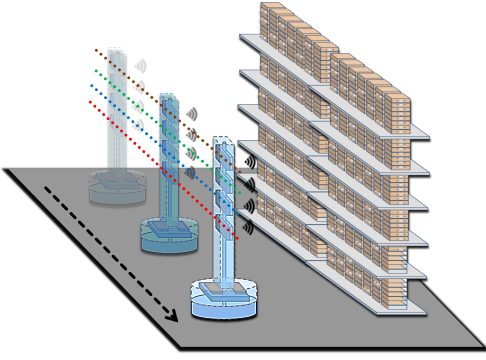


Fig. 5: Sketch of a localization scenario. Four antennas mounted on each side of a moving robot form a multi-antenna synthetic aperture

the global path the robot calculated to follow may be totally invalid, thus fast modifications may be performed so as to reach the goal in safety. Furthermore, usually motion-commands' translation to robot velocities is never accurate, due to mechanical inconsistencies in the robot's motion system, slippages or frictions of the wheels or even due to environmental culprits. Finally, in the 2D case, there is the lack of information around the vertical dimension. Consider for instance the case where a table resides in the environment, and navigation is performed only through the use of a LIDAR sensor: the map of the environment may only contain information about the legs of the table, which means that the navigation module may instruct the robot to pass *through* the table rather than around it, causing it to crash. This danger is more pronounced when the robot is an aerial one and the environment features different obstacles at different heights. Similarly, poor pose estimation may result in crashes because the navigation's local planner relies upon accurate pose estimates.

III. LOCALIZATION OF RFID TAGS

A. Robot-Location-Aware Methods

The robot moves along a straight path and carries four antennas per side (8 antennas in total), each of which is forming a synthetic aperture at a different height, as demonstrated in Fig. 5. In order to solve the problem of localizing a tag in the 3D space, each antenna and its measurements are initially treated independently. For each antenna, we assume the tag to be located at the same height as the antenna. This relaxes the problem in two dimensions. We will actually find the radius of a circle, perpendicular to the line of motion, where the tag may-be located. When multiple circles introduced by additional antennas are combined, the equivalent 3D locus is reduced to a single point. The tag's location is finally released on the intersection of those circles and determined in a least-squared sense.

1) **Phase ReLock**: For the 2D problem, consider an antenna taking phase measurements θ_i along a straight synthetic

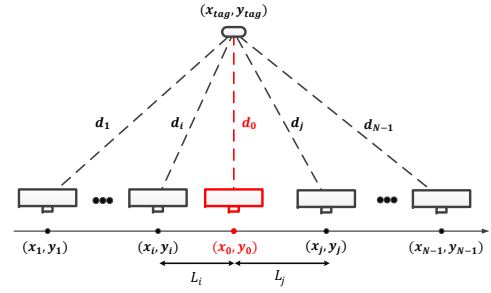


Fig. 6: Geometry of the two-dimensional problem

aperture consisted of N positions (x_i, y_i) , as depicted in Fig. 6. The theoretical phase model can be expressed as

$$\phi_i = \left(\frac{4\pi}{\lambda} d_i(x_{tag}, y_{tag}) + c_{tag} \right) \bmod 2\pi, \quad i \in [0, N-1] \quad (2)$$

where d_i is the distance between the tag and the i^{th} antenna location and c_{tag} corresponds to the additional phase offset introduced by the tag's and the reader's electronics. This term is considered constant for each RFID antenna-tag pair, but yet unknown.

In general, our target is to find the values of the unknown parameters of model (2) so that the expected values ϕ_i best match the measured θ_i . This is a common problem of data fitting and is solved by minimizing the following least squared-based objective function:

$$F(x_{tag}, y_{tag}, c_{tag}) = \sum_{i=0}^{N-1} [\phi_i - \theta_i]^2 \quad (3)$$

(3) is a non linear model with unknown coefficients $(x_{tag}, y_{tag}, c_{tag})$. In most cases a closed-form solution is not feasible and iterative algorithms are deployed [34]- [35]. Such algorithms iteratively converge to a minimum of the corresponding objective function.

It was demonstrated in [12] and [13], that (3) does not converge to the optimum solution; instead the algorithm is trapped to a local minimum, due to the nature of the objective function, demonstrated in Fig. 7 - left. In order to avoid the solution of a time consuming grid-based search, we perform phase unwrapping. The new objective function has a single minimum as shown in Fig. 7 - right. Rapid convergence to the best solution is now feasible, provided that the initial point of the algorithm belongs to the subspace the antenna is facing to.

By computing the perpendicular distance d_0 from (x_{tag}, y_{tag}) to the antenna's path-line, one defines the 3D locus of possible tag locations. Then, for the 3D solution, all points that are located at distance d_0 from (x_0, y_0, z_0) , and lay on the plane that crosses (x_0, y_0, z_0) and is perpendicular to the antenna's path, are equally likely to be the tag's true location (z_0 corresponds to the antenna's known height). Hence, the locus is a circle with center (x_0, y_0, z_0) , radius d_0 and normal vector that is parallel to the antenna's trace (see Fig. 8 left).

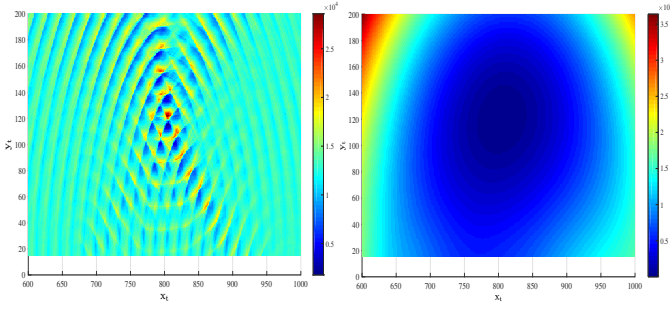


Fig. 7: Objective function (3) for original data (left) and after phase unwrapping (right). Red and blue colors denote high and low amplitudes of (3), respectively.

2) **Min Distance Model:** A new approach of rapidly solving the localization problem is proposed here. Consider the straight antenna array of Fig. 6. Let (x_0, y_0) denote the antenna position that corresponds to the minimum tag-to-antenna distance. Since the antenna is moving along a straight path, the tag should be located on the line that joins (x_{tag}, y_{tag}) and (x_0, y_0) , and is perpendicular to the antenna's path-line. That position is identified as the location at which the minimum value of the unwrapped phase-curve was recorded. Considering (x_0, y_0) as a reference point, for the rest $N - 1$ antenna's positions, we define the differences of the tag-to-antenna distances as

$$\Delta d_i = \frac{\lambda}{4\pi} \Delta \theta_i, \quad i \in [1, N - 1] \quad (4)$$

where $\Delta d_i = d_i - d_0$, $\Delta \theta_i = \theta_i - \theta_0$ and d_0 is the distance between the tag and the reference point; d_0 is considered the *unknown parameter* of the problem.

Due to the periodicity of the measured phase-curve, any measurement could correspond to more than one spatial distances between the tag and the antenna. In fact, each value θ_i corresponds to $d_i + k\frac{\lambda}{2}$. So the actual distance differences Δd_i cannot be directly computed, unless phase unwrapping is performed and unwrapped data are used. Furthermore, according to Pythagorean Theorem applied on Fig. 6:

$$\Delta d_i = \sqrt{d_0^2 + L_i^2} - d_0, \quad i \in [1, N - 1] \quad (5)$$

where L_i is the distance between each antenna location from the reference point (x_0, y_0) . After simple operations and substitutions, the result is an overdetermined linear system

$$2\Delta d_i d_0 = L_i^2 - \Delta d_i^2, \quad i \in [1, N - 1] \quad (6)$$

Denoting $a_i = 2\Delta d_i$ and $b_i = L_i^2 - \Delta d_i^2$, the objective function of the least square problem is

$$F(d_0) = \sum_{i=1}^{N-1} [a_i d_0 - b_i]^2 \quad (7)$$

In contrast to non linear problems, linear ones can be expressed by closed forms and solved by simple matrix operations. The solution is derived by differentiating (7) with respect to

coefficient d_0 , and then setting the result equal to zero [36], [37]. The 3D locus is finally defined similarly as in the non linear case.

3) **Loci Intersection:** Solving the two dimensional problem by each of the four antennas, results in the introduction of four circles, as shown in Fig. 8 (left). The final locus is thus, reduced to a unique point; i.e. the intersection point of the circles. However in practice, all circles are not expected to intersect at a single point, since they have been computed with some error. Therefore, a weighted least square solution is given to the intersection problem.

Without loss of generality, x-axis is defined to coincide with the robot's path. For better representation, the $x - y$ and $y - z$ planes are reconstructed in Fig. 8 - (middle) and (right), respectively. In general, the circles are not expected to lay at the same plane (as shown in Fig. 8 - middle), but at least, they have identical normal vectors, parallel to the robot's path. Therefore, the x coordinate of the tag is estimated by

$$x_{tag} = \frac{\sum_{i=1}^4 \hat{x}_i}{4} \quad (8)$$

while the y and z coordinates correspond to the least squared solution of the following non-linear system

$$(\hat{y}_i - y_{tag})^2 + (\hat{z}_i - z_{tag})^2 = R_i^2, \quad i \in [1, 4] \quad (9)$$

where $(\hat{x}_i, \hat{y}_i, \hat{z}_i)$ is the center C_i of the i^{th} circle and R_i its radius (see Fig. 8-right).

B. Robot-Agnostic Methods

In [16], [17], we presented an improved version of the classical "Landmark" [15] localization algorithm. Reference tags are placed at known locations in the target area. As each reader antenna, mounted on top of the robots or drone, collects measurements of both target and reference tags, the algorithm builds a metric, where the sum of the differences between the measured samples of the target tags minus the corresponding ones of the reference tags are evaluated:

$$D_l^j = \sqrt{\sum_{i=1}^N (X_i^j - R_i^l)^2 / N} \quad (10)$$

In (10), for each robot-antenna location i , where *both* the reference tag l and the target tag j have been measured, the corresponding difference between their RSSI or unwrapped phase values is added to the "resemblance" metric D_l^j between the specific two tags. The location of each tracked tag is calculated according to the normalized weighted sum of the coordinates of the k-nearest reference tags, after sorting (10) with respect to j , [16], [17].

In addition to the standard "Landmark", we treat the reference tags also as unknowns and also estimate their locations. Exploitation of the reference tags in such manner gave two advantages: *i*) a set of parameters, related to the execution of the algorithm is fine-tuned during the experiment, so that the localization error of the reference tags (which can be calculated, since the locations are known), is minimized *ii*) the

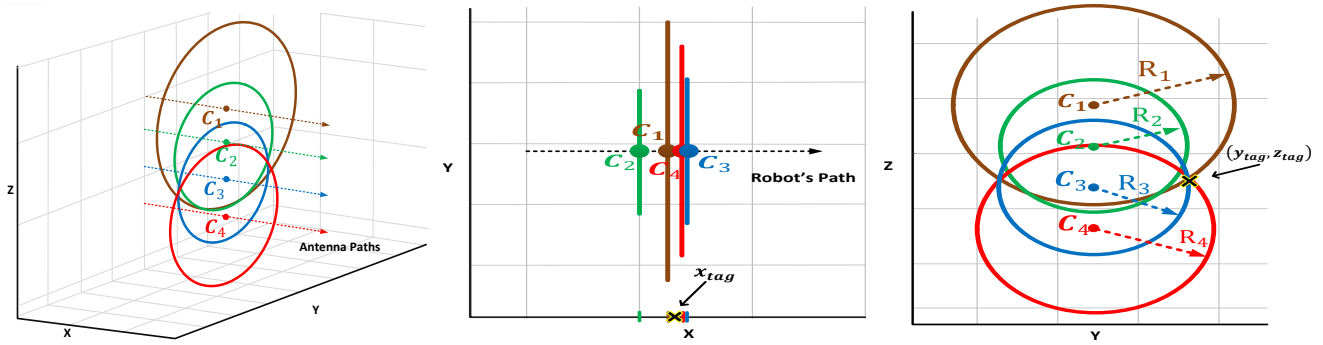


Fig. 8: Left - The equivalent 3D locus produced by four antennas. Middle - The representation of X-Y plane. Right - The representation of the Y-Z plane

mean achieved localization-accuracy can be evaluated, which is a very valuable information for commercial applications, since the robot can be instructed to pass again through areas, where poor accuracy has been recorded. Furthermore, pairs of target-reference tags with few common (from the same antenna location) samples are discarded from the estimations. The fingerprinting algorithms are used on the drone, where accurate estimation of its location in the map is not possible. The drone is destined mainly for flying above the target area (inventorying horizontal storage, like buildings' materials, woods, etc.).

IV. MEASUREMENTS

The measurements were conducted inside a laboratory environment, as shown in Fig. 9. 100 passive UHF RFID tags were attached on top of two roll-up banners and 100 tags on top of a long desk. Their relative position on each banner was known, since the tags were attached on millimeter paper. The banners were then moved in different positions and orientations inside the area, in order to investigate the effect of different propagation conditions, different tags' densities per m^3 , etc. As the robot moved in the area, it constructed an accurate 2D map of the environment, demonstrated in Fig. 4 (left) and a less accurate 3D map, demonstrated in Fig. 4 (right).

In order to evaluate the accuracy of the proposed methods, we need to pinpoint the locations of the banners inside the 2D map, such that the local coordinate system of the banner is transformed to the coordinate system of the robot. This manual process is not necessary in the actual inventorying application, since the results are directly shown in the map created by the robot, but only for evaluation of the accuracy of the different methods. This manual process is expected to add an error in the order of 5cm. The results are summarized in Table I.

"Phase ReLock" outperformed the other two methods, achieving mean error around 25cm in all experiments, while processing approximately 100000 measured samples from 100 tags in just 12s. The achieved accuracy is impressive, considering that the robot's trace was not known (but estimated), the considered actual locations of the tags (ground truth) might suffer from errors in the order of cm, the environment is



Fig. 9: Representation of the measurements set-up. The banners have been placed side by side (Left) and back-to-back (Right)

full of scatterers (multipath-rich), the solution was sought in 3D space and not along a given horizontal cut. The fingerprinting method achieved an acceptable accuracy. 44 out of 100 tags were used as reference, having a density of 22 reference tags/ m^3 , which is a rather big number for commercial applications. The new "Linear" approach was the fastest, but less accurate than "Phase ReLock", due its constraint of "identifying" a single point on the trace of the robot, for which the distance to the tag was minimized.

V. CONCLUSIONS

In this paper, we have presented our latest findings on the complex problem of autonomous inventorying and localization of RFID tags by a moving robot. To the best of our knowledge, this is the first paper that deals jointly with the necessary sub-problem of map-construction, localization of the robot, navigation and localization of the tags. We have presented three algorithms, which can be applied for real-time tag localization and compared their performance in realistic configurations. 3D experimental results demonstrated 25cm mean accuracy for dense tag populations in a multipath-rich environment. Though further improvement can be accomplished, the achieved 3D accuracy is sufficient for most inventorying applications in large warehouses or retail stores, except perhaps for pick-and-place robots, where mm accuracy is desired.

TABLE I: Experimental Results

Experiment	Phase ReLock			Min-Distance Model			Fingerprinting Phase			Fingerprinting RSSI		
	mean error (cm)	std (cm)	cost (sec)	mean error (cm)	std (cm)	cost (sec)	mean error (cm)	std (cm)	cost (sec)	mean error (cm)	std (cm)	cost (sec)
Back to Back (100 tags)	26.2	33.9	12.6	29.7	29.7	6	42	23.5	42	42	23.4	42
Side by Side (100 tags)	23.4	25.2	13.8	32.2	29.8	7.4	43.3	29	32	42.5	27.8	32
Single Banner (50 tags)	25.3	24.6	6.9	36.4	37	3.1	19.4	13.1	43	20.8	12.3	43
Single B-Horizontal (50 tags)	27.5	29	4.9	34.5	33.8	2.8	38	26.6	62	37.3	24.5	62
All experiments	25.3			32.4			38			37.8		

REFERENCES

- [1] RELIEF project, "http://relief.web.auth.gr/", last accessed on January 9 2020.
- [2] Tory-robot, "Metralabs", "https://www.metralabs.com/en/rfid-robotory/", last accessed on January 9 2020.
- [3] AdvanRobot, "Keonn", "https://www.keonn.com/systems/view-all-2/inventory-robots.html", last accessed on January 9 2020.
- [4] StockBot, "Pal Robotics", "http://pal-robotics.com/robots/stockbot/", last accessed on January 9 2020.
- [5] R. Miesen, F. Kirsch, and M. Vossiek, "UHF RFID localization based on synthetic apertures," *IEEE Transactions on Automation Science and Engineering*, vol. 10, no. 3, pp. 807-815, 2013.
- [6] L. Yang, Y. Chen, X.-Y. Li, C. Xiao, M. Li, and Y. Liu, "Tagoram: real-time tracking of mobile rfid tags to high precision using cots devices," In *Proceedings of the 20th annual international conference on Mobile computing and networking*, pp. 237-248, 2014.
- [7] L. Shanguan and K. Jamieson, "The design and implementation of a mobile rfid tag sorting robot," In *Proceedings of the 14th Annual International Conference on Mobile Systems, Applications, and Services*, pp. 31-42, 2016.
- [8] A. Motroni, P. Nepa, P. Tripicchio, M. Unetti, "A Multi-Antenna SAR-based method for UHF RFID Tag Localization via UGV", 2018 IEEE International Conference on RFID Technology & Application (RFID-TA), Macau, China, 2018.
- [9] E. DiGiampaolo, F. Martinelli, "A Robotic System for Localization of Passive UHF-RFID Tagged Objects on Shelves," *IEEE Sensors Journal*, vol. 18, no. 20, pp. 8558-8568, 2018.
- [10] J. Wang and D. Katabi, "Dude, where's my card?: RFID positioning that works with multipath and non-line of sight," *Proceedings of the ACM SIGCOMM 2013 conference on SIGCOMM*, Hong kong, China, pp. 51-62, 2013.
- [11] Y. Ma, N. Selby, F. Adib, "Minding the billions: ultra-wideband localization for deployed RFID tags," *MobiCom 2017, 23rd Annual Conference on Mobile Computing and Networking*, Utah, USA, 2017.
- [12] A. Tzitzis, S. Megalou, S. Siachalou, T. Yioultsis, A. Kehagias, E. Tsardoulis, A. Filotheou, A. Symeonidis, L. Petrou and A. G. Dimitriou, "Phase ReLock - Localization of RFID Tags by a Moving Robot," 13th European conference on Antennas and Propagation, Krakow, Poland, 2019.
- [13] A. Tzitzis, S. Megalou, S. Siachalou, E. Tsardoulis, A. Kehagias, T. Yioultsis, A. G. Dimitriou, "Localization of RFID Tags by a Moving Robot, via Phase Unwrapping and Non-Linear Optimization," *IEEE Journal of Radio Frequency Identification*, vol 3, no. 4, pp. 216-226, Dec. 2019.
- [14] A. Tzitzis, S. Megalou, S. Siachalou, E. Tsardoulis, T. Yioultsis, A. G. Dimitriou, "3D Localization of RFID Tags with a Single Antenna by a Moving Robot and Phase ReLock," 2019 IEEE International Conference on RFID-Technology and Applications, RFID-TA 2019, Pisa, Italy, September 2019.
- [15] L. M. Ni and Y. Liu, "LANDMARC: indoor location sensing using active RFID," *Wireless Networks*, 10(6), pp. 701-10, 2004.
- [16] S. Megalou, A. Tzitzis, S. Siachalou, T. Yioultsis, J. Sahalos, E. Tsardoulis, A. Filotheou, A. Symeonidis, L. Petrou, A. Bletsas, A. G. Dimitriou, "Fingerprinting Localization of RFID tags with Real-Time Performance-Assessment, using a Moving Robot," 13th European Conference on Antennas and Propagation, Krakow, Poland, March 2019.
- [17] S. Siachalou, S. Megalou, A. Tzitzis, E. Tsardoulis, A. Bletsas, J. Sahalos, T. Yioultsis, A. G. Dimitriou, "Robotic Inventorying and Localization of RFID Tags, Exploiting Phase-Fingerprinting," 2019 IEEE International Conference on RFID-Technology and Applications, RFID-TA 2019, Pisa, Italy, September 2019.
- [18] Zhang, Zhengyou, "Microsoft Kinect Sensor and Its Effect", in *IEEE MultiMedia*, vol. 19, pp. 4-12, IEEE Computer Society
- [19] Thrun, Sebastian and Burgard, Wolfram and Fox, Dieter, "Probabilistic Robotics", 2005, The MIT Press
- [20] Park, Sangheon, and Yu, Sunjin, and Kim, Joongrock, and Kim, Sungjin, and Lee, Sangyoun. "3D hand tracking using Kalman filter in depth space". *EURASIP Journal on Advances in Signal Processing*. 2012.
- [21] Alhwarin, Faraj, Ferrein, Alexander and Scholl, Ingrid. "IR Stereo Kinect: Improving Depth Images by Combining StructuredLight with IR Stereo", *PRICAI 2014: Trends in Artificial Intelligence*, 2014, Springer International Publishing.
- [22] Vit, Adar and Guy Shani. "Comparing RGB-D Sensors for Close Range Outdoor Agricultural Phenotyping.", *Sensors*, 2018.
- [23] M. Paton and J. Kosecka, "Adaptive RGB-D Localization," Ninth Conference on Computer and Robot Vision, Toronto, ON, 2012, pp. 24-31
- [24] Loianno, Giuseppe and Lippiello, Vincenzo and Siciliano, Bruno, "Fast localization and 3D mapping using an RGB-D sensor". 2013, 16th International Conference on Advanced Robotics, ICAR 2013. 1-6. 10.1109/ICAR.2013.6766558.
- [25] Maybeck, Peter S., "Stochastic models, estimation, and control, Volume 141, "Mathematics in Science and Engineering", 1979
- [26] Sebastian Thrun. "Particle filters in robotics". In *Proceedings of the Eighteenth conference on Uncertainty in artificial intelligence (UAI'02)*. Morgan Kaufmann Publishers Inc., San Francisco, CA, USA, 511-518.
- [27] Fox, D. "Adapting the Sample Size in Particle Filters Through KLD-Sampling". *The International Journal of Robotics Research*, 2003, 22(12), 985-1003. <https://doi.org/10.1177/0278364903022012001>
- [28] F. Dellaert, D. Fox, W. Burgard and S. Thrun, "Monte Carlo localization for mobile robots," *Proceedings 1999 IEEE International Conference on Robotics and Automation (Cat. No.99CH36288C)*, Detroit, MI, USA, 1999, pp. 1322-1328 Volume 2, doi: 10.1109/ROBOT.1999.772544
- [29] Hornung, A., Wurm, K.M., Bennewitz, M. et al. (2013). "OctoMap: an efficient probabilistic 3D mapping framework based on octrees". *Autonomous Robots* 34 (3): 189-117.
- [30] Filotheou, A., Tsardoulis, E., Dimitriou, A. et al. "Quantitative and Qualitative Evaluation of ROS-Enabled Local and Global Planners in 2D Static Environments". *Journal of Intelligent Robotic Systems* (2019) doi:10.1007/s10846-019-01086-y
- [31] Jean-Claude Latombe, "Robot Motion Planning", 1991.
- [32] C. Rosmann, W. Feiten, T. Wösch, F. Hoffmann and T. Bertram, "Trajectory modification considering dynamic constraints of autonomous robots". *Proc. 7th German Conference on Robotics*, Germany, Munich, 2012, pp 74-79.
- [33] C. Rosmann, W. Feiten, T. Wösch, F. Hoffmann and T. Bertram, "Efficient trajectory optimization using a sparse model". *Proc. IEEE European Conference on Mobile Robots*, Spain, Barcelona, 2013, pp. 138-143.
- [34] R. H. Byrd, R. B. Schnabel, and G. A. Shultz, "Approximate Solution of the Trust Region Problem by Minimization over Two-Dimensional Subspaces," *Mathematical Programming*, vol. 40, pp. 247-263, 1988.
- [35] V. Buljak, "Optimization Algorithms" in *Inverse Analyses with Model Reduction*, 1st Ed., 2012.
- [36] R. Penrose, "A generalized inverse for matrices," *Mathematical Proceedings of the Cambridge Philosophical Society*, vol.51, no. 3, pp. 406-413, 1955.
- [37] C. R. Goodall, "Computation using the QR decomposition," in *Handbook of Statistics*, vol. 9, pp. 467-508, 1993.